HHS Public Access

Author manuscript

Brain Res. Author manuscript; available in PMC 2022 July 05.

Published in final edited form as:

Brain Res. 2020 January 15; 1727: 146569. doi:10.1016/j.brainres.2019.146569.

The Ubiquitin-Editing Enzyme A20 Regulates Synapse Remodeling and Efficacy

Shaolin Mei[1], **Hongyu Ruan**[2], **Qi Ma**[2,*], **Wei-Dong Yao**[1,2,*]

[1]Program in Neuroscience, State University of New York, Upstate Medical University, Syracuse, NY 13210

[2]Department of Psychiatry and Behavioral Sciences, State University of New York, Upstate Medical University, Syracuse, NY 13210

Abstract

Ubiquitination and its reverse process, deubiquitination, play essential roles in neural development, function, and plasticity. A20, a ubiquitin editing enzyme that can remove K63-polyubiquitin chains from substrates and attach K48-polyubiquitin chains to them, is a critical component in the NF-κB signaling pathway in the immune system. This dual ubiquitin enzyme is also present in mammalian brains, but its potential role in neurons and synapses is unknown. We show that A20 in pyramidal neurons potently regulates dendritic arborization, spine morphogenesis, and synaptic transmission through an NF-κB-dependent mechanism. In cultured hippocampal neurons, overexpression of A20 reduced dendritic complexity and spine size and density, whereas A20 knockdown increased spine size and density, as well as clustering of the postsynaptic scaffold PSD-95 and glutamate receptor subunit GluA1. A20 effects in vitro were recapitulated in vivo where increasing or decreasing A20 expression in mouse brains reduced and enhanced spine density, respectively. Functionally, A20 knockdown significantly increased the amplitude, but not frequency of miniature excitatory postsynaptic currents, suggesting a role in postsynaptic efficacy. A20 negatively regulated NF-κB activation in neurons and A20 mutants deficient in either the deubiquitinase or the ubiquitin ligase activity failed to suppress NF-κB activation or reduce spine morphogenesis. Finally, selective inhibition of NF-κB abolished A20 knockdown-elicited spine formation, suggesting that A20 exerts its modulation on synapses through NF-κB signaling. Together, our study reveals a previously unknown role for A20, the only known ubiquitin editing enzyme with both deubiquitinase and ubiquitin ligase activity, in dendritic arborization, spine remodeling, and synaptic plasticity.

Keywords

Dendritic spines; synapse remodeling; ubiquitination; deubiquitinase; ubiquitin ligase; NF-κB

*To whom correspondence should be addressed: Wei-Dong Yao, Ph.D. (yaow@upstate.edu), Qi Ma, Ph.D. (maq@upstate.edu), SUNY Upstate Medical University, 750 E. Adams St, Syracuse, NY 13210, Ph: 315-464-3194, Fax: 315-464-3155.

1. Introduction

Protein ubiquitination plays important roles in neural development and synapse and circuit plasticity, with major implications in various neurological and psychiatric diseases (Bingol and Sheng, 2011; George et al., 2018; Harper et al., 2018; Mabb and Ehlers, 2010; Yamada et al., 2013). The conjugation of ubiquitin(s) to a substrate is catalyzed by sequential actions of E1 (ubiquitin-activating), E2 (ubiquitin-conjugating), and E3 (ubiquitin ligases) enzymes (Hershko and Ciechanover, 1998). This process is reversed by deubiquitination, catalyzed by a large and diverse deubiquitinase (DUB) family including ubiquitin-specific proteases, ovarian tumor (OTU) enzymes, Machado-Josephin domain enzymes, and ubiquitin C-terminal hydrolases (Komander et al., 2009). The function of ubiquitination is largely determined by ubiquitin linkage topologies: K48-linked ubiquitination generally directs substrates to proteasome-dependent degradation, whereas K63-linked ubiquitination is non-degradable and regulates signaling activation, endocytosis, and protein interactions (Chen and Sun, 2009; Haglund and Dikic, 2005; Husnjak and Dikic, 2012; Mukhopadhyay and Riezman, 2007). Many studies have established the ubiquitin-proteasome system (UPS) as a major mechanism in activity-dependent synapse deconstruction and remodeling, as a result of UPS-mediated protein degradation and turnover (Bingol and Sheng, 2011; DiAntonio and Hicke, 2004; Mabb and Ehlers, 2010). In addition, emerging studies point to an essential role of K63-linked ubiquitination in synapse formation and plasticity (Ma et al., 2017). Specifically, the scaffolding protein postsynaptic density-95 (PSD-95) is conjugated with K63 polyubquitin chains by the E3 ligase TNF receptor-associated factor 6 (TRAF6), which promotes PSD-95 scaffolding and maturation of synapses (Ma et al., 2017).

A20, also known as tumor necrosis factor α-induced protein 3 (TNFAIP3), belongs to the OTU family of DUBs. A20 is unique because it possesses both K63-linked deubiquitination activity and K48-linked ubiquitin ligase activity: in addition to acting as a standard E3 or DUB that targets separate substrates, it can remove K63-polyubiquitin (polyUb) chains from some substrates and subsequently attach K48-polyUb chains to the same substrates, thus displaying a rare ubiquitin chain editing capability (Shembade et al., 2010; Wertz et al., 2004). A20 contains 790 amino acid residues and harbors one OTU domain and seven zinc finger motifs (Bosanac et al., 2010; Ma and Malynn, 2012; Skaug et al., 2011). A20 plays important roles in immune and inflammation responses through negative modulation of NF-κB activation by antagonizing several key players (Catrysse et al., 2014; Ma and Malynn, 2012; Vereecke et al., 2009). Specifically, A20 removes K63-polyUb chains from RIP1 (receptor-interacting protein 1), TRAF2, TRAF6, and NEMO (NF-κB essential modulator, also known as inhibitor of nuclear factor kappa-B kinase subunit gamma (IKK-γ)), and adds K48-polyUb chains to RIP1, NEMO and UBC13 (ubiquitin-conjugating enzyme E2 13) to promote their proteasome-dependent degradation, leading to inhibition of NF-κB activation (Ma and Malynn, 2012; Shembade et al., 2010; Wertz et al., 2004). In the CNS, it has been shown that A20 ubiquitin editing complex is expressed in neurons in the human brain (Pranski et al., 2012), and limited studies suggest that A20 plays a role in neuroinflammation and neurodegeneration (Guedes et al., 2014; Parisi et al., 2016; Peluffo et al., 2013; Wang et al., 2013; Yu et al., 2006). Whether or not A20 expressed in neurons regulates synapse function and plasticity is unknown.

In the present study, we first characterized the temporal, tissue, and subcellular expression profiles of A20 in rodent brains and neurons. We then manipulated the levels of A20 in hippocampal neurons in vitro and in vivo and investigated the effects in dendritic arborization, spine morphogenesis, and synaptic strength. We finally evaluated the potential role of the neuronal NF-κB signaling in this process. Our results demonstrate that A20 in pyramidal neurons potently regulates dendritic spine remodeling and synaptic efficacy via an NF-κB-dependent mechanism.

2. Results

2.1 A20 expression profiles in rodent neurons

We first examined A20 expression in cultured rat cortical neurons during development by Western blotting. We detected the expected 82 kDa band for A20, which appeared at DIV (days in vitro) 1 and became intensified gradually thereafter and peaked at DIV 17 (Fig.1A-B). This developmental profile roughly paralleled the expression pattern of PSD-95, a major postsynaptic scaffolding protein in excitatory synapses. To confirm A20 expression in the brain, we repeated above Western blotting experiments on mouse cortical lysates prepared from different postnatal (P) days. Cortical A20 expression also displayed progressive increase through P30 and a largely similar developmental profile to cortical PSD-95 (Fig. 1C–D). To gain insights about A20 subcellular expression in neurons, we obtained subcellular fractions from adult rat brain and detected A20 levels in different fractions. We found that A20 was present in all purified fractions but showed an enrichment in the postsynaptic density (PSD), and a relative lack of expression in the presynaptic fraction (Fig.1E). Finally, we performed immunostaining and fluorescence microscopy on cultured rat hippocampal neurons to visualize the subcellular localization of A20 in neurons. Co-staining of endogenous A20 and PSD-95 revealed that A20 indeed was expressed throughout individual neurons and displayed substantial co-localization with PSD-95 (Fig. 1F).

Since above experiments depended on antibody specificity, we performed two experiments to ensure the specificity of the commercially available A20 antibody (Fig. S1). First, immunoblotting of endogenous A20 and ectopically expressed Myc-A20 and GFP-A20 in transfected HEK293T cells using the A20 antibody clearly showed specific Myc-A20, GFP-A20 and endogenous A20 protein bands, as well as the expected higher A20 levels in overexpressed cells (Fig. S1A). Second, immunofluorescence experiments showed that the endogenous A20 signal was significantly lower in neurons transfected with a shA20 sequence (coexpressing GFP; see Fig. 3B below for shA20 knockdown efficiency) compared to adjacent non-transfected neurons on the same coverslip, or to neurons transfected with the control shRNA sequence, shLuc/GFP (Fig. S1B,C). Thus, the A20 antibody we used was specific. Taken together, our results indicated that A20 is expressed in neurons in a development-dependent manner and is associated with the PSD at excitatory synapses.

2.2 A20 negatively regulates dendrite complexity and spine morphology in cultured hippocampal neurons

To explore the role of A20 in neurons and synapses, we first examined whether A20 affects dendritic arborization and spine morphology. Cultured rat hippocampus neurons were transfected with DsRed-A20 or the DsRed control vector (Fig. 2A) at DIV7, and neuronal morphology was analyzed at DIV19. Neurons expressing DsRed-A20 appeared generally healthy based on their overall morphology (Fig. 2B). Sholl analysis indicated that exogenous expression of DsRed-A20 reduced the neurite complexity, especially at medial-distal sections of the dendritic tree (Fig. 2B, C). Specifically, dendritic branches and arborization approximately between 100 and 250 μm away from the soma displayed less complexity in neurons transfected with DsRed-A20 compared to DsRed (Fig. 2B, C). Analysis of dendritic spines revealed that A20 overexpression markedly and similarly reduced spine density across proximal, medial, and distal processes (Fig. 2D, E). Further characterizations of different spine types showed that A20 overexpression did not change the proportions of mushroom, stubby, and thin spines (Fig. 2F), but significantly decreased the size and density of all three types, resulting in an overall loss of total dendritic spines (Fig. 2G-I).

We next examined how A20 down-regulation affects neuronal morphogenesis using RNAi. We designed three shRNA sequences against rodent A20 and tested their knockdown efficiencies in transfected HEK293FT cells. shRNA #1 and #2 (but not #3) reduced exogenously expressed Myc-A20 (mouse) by ~50% compared to the shLuc control (Fig. 3A,B), but did not affect the level of endogenous A20 (human) (Fig. 3C,D), indicating shRNA#1 and #2 are selective and effective. In subsequent experiments, we used shRNA#1 (designated shA20) because it has sequence homology to both mouse and rat A20 and can be used for both mouse and rat neurons. When transfected into hippocampal neurons, shA20 did not overly affect dendritic complexity (Fig. 3E, F). A20 knockdown also did not noticeably alter the proportions of mushroom, stubby, and thin spines (Fig. 3G, H). However, A20 knockdown significantly increased total spine density (Fig. 3J) as well as the size (Fig. 3I) and density (Fig. 3K) of mushroom and stubby spines. Importantly, the shA20-induced increase in mushroom spine size as well as increases in total, mushroom, and stubby spine densities were rescued by co-expressing an RNAi-resistant human A20 (Fig. 3I-K). These results are generally consistent with above A20 overexpression data and support a role for A20 in negatively regulating dendritic spine morphogenesis.

2.3 A20 regulates dendritic spine densities in vivo

To investigate whether A20 remodels dendritic spines in vivo, we generated a series of lentivirus that express GFP (as control), A20/GFP, shLuc/GFP, or shA20/GFP (Fig. 4A). When tested in cultured neurons, A20/GFP virus significantly increased A20 protein level compared to GFP virus, whereas shA20/GFP virus significantly reduced A20 level compared to shLuc/GFP virus (Fig. 4B). We injected each virus into the hippocampi of P15 mice and sacrificed the mice at P30, and their brains were fixed and sectioned for dendritic spine analysis. The densities of total, mushroom, and stubby spines were all significantly reduced by A20 overexpression in infected CA3 neurons (Fig. 4C, D, G). In contrast, A20 knockdown increased the densities of total, mushroom and stubby spines (Fig. 4E, F, H).

These results confirmed the role of neuronal A20 in remodeling dendritic spines in the intact mouse brain.

2.4 A20 decreases the expression and clustering of PSD-95 and GluA1

We next examined how A20 regulates the level and clustering of the α-amino-3-hydroxy-5-methyl-4-isoxazolepropionic acid (AMPA) glutamate receptor subunit GluA1, the major subunit forming synaptic and extrasynaptic AMPARs (Lu et al., 2009; Traynelis et al., 2010; Wenthold et al., 1996), and the synaptic scaffold PSD-95 in cultured hippocampal neurons. Overexpressing A20/GFP significantly reduced the protein levels of PSD-95 and GluA1 (Fig. 5A). In contrast, knocking down A20 significantly increased PSD-95 and GluA1 levels (Fig. 5B). Immunofluorescence confocal microscopy showed that A20 knockdown significantly increased the intensity of PSD-95 clusters (Fig. 5C, F). In addition, the cluster intensities of both surface and total GluA1 were increased in A20 knockdown neurons (Fig. 5D-F). These data are consistent with the “slot hypothesis” (Elias and Nicoll, 2007) that PSD-95 serves as a postsynaptic slot scaffold that controls GluA1 numbers at synapses. Taken together, our results suggest that A20 negatively regulates synapse maturation and/or function.

2.5 A20 knockdown increases synaptic strength

To directly investigate whether A20 regulates synaptic strength, we performed whole-cell patch-clamp recordings on infected rat hippocampus neurons and measured the amplitude and frequency of AMPA receptor-mediated miniature excitatory postsynaptic currents (mEPSCs). A20 knockdown significantly increased mEPSC amplitude (Fig. 6A, B, C), indicating a larger number of postsynaptic AMPA receptors and/or an increased presynaptic release probability. However, the mEPSC frequency, an index of presynaptic release probability or the number of functional synapses, remained unchanged (Fig. 6A, D, E). Importantly, co-expression of the RNAi-resistant A20 rescued mEPSC amplitude increase (Fig. 6A, B, C). Thus, these results indicate that A20 knockdown promotes synaptic strength, likely resulting from higher postsynaptic AMPA receptor contents.

2.6 A20 suppresses constitutive NF-κB activation in neurons

To illustrate the potential mechanisms by which A20 remodels the synapses, we focused on the transcription factor NF-κB which plays important roles in synaptic remodeling and plasticity (Meffert and Baltimore, 2005). A20 is a well-known negative regulator of NF-κB signaling through deubiquitination/ubiquitination-mediated suppression of several NF-κB activators (Wertz et al., 2004). In agreement with previous studies that NF-κB is constitutively active in neurons (Kaltschmidt and Kaltschmidt, 2009), characterized by a high level of phosphorylated p65 (p-p65), we detected abundant p-p65 Ser536 in our cultured neurons (Fig. 7A). Western blotting indicated that A20 overexpression significantly reduced total levels of UBC13, phosphorylated IκBα S32, p65, and phosphorylated p65 S536, indicating effective suppression of the NF-κB activation by A20 in cultured neurons (Fig. 7B, C). In contrast, A20 knockdown significantly increased phosphorylated p65 S536 in cultured neurons (Fig. 7B, C). Thus, these results confirm that A20 negatively regulates NF-κB activation in neurons, similar to its role in non-neuronal cells (Chen, 2005).

Phosphorylation of p65 S536 is considered a key signal of NF-κB activation and is important for NF-κB-promoted neuronal morphogenesis (Gutierrez et al., 2008). To confirm that A20 regulates p-p65 S536 in individual neurons, we measured the fluorescence intensity of p65 and p-p65 S536 staining in transfected cultured hippocampal neurons (Fig. 7D). A20 overexpression significantly reduced p65 and p-p65 S536 intensities, whereas A20 knockdown drastically increased p-p65 S536 level. Cysteine to alanine mutations at either C103 (essential to A20 deubiquitination activity) or C624 and C627 (required for the E3 ligase activity of A20) abolished the inhibition of p65 and p-p65 S536 by wild-type A20 (Fig. 7D, E). These data suggest that both DUB activity and the E3 ligase activity of A20 are required for its full effects on p65 and p-p65 S536 in neurons.

We next used a luciferase reporter assay to further confirm the modulation of NF-κB activation by A20 in neurons. High density cultured hippocampal neurons were co-transfected with NF-κB-Luciferase, TK-Renilla, and indicated A20 constructs (Fig. 8A). Luciferase activity quantifications showed that overexpression of wild-type A20, but not C103A or C624/C627A mutants significantly reduced NF-κB activation, whereas A20 knockdown increased NF-κB activation (Fig. 8A).

To directly observe A20 modulation of NF-κB activation in individual neurons, we used the fluorescence-based IκB-HcRed reporter (Wang et al., 2010), which when transfected into cultured neurons can indicate NF-κB activation. HcRed fluorescence quantifications showed that ectopic expression of wild-type A20, but not C103A or C624/C627A significantly reduced HcRed fluorescence (an indicator of NF-κB activation) (Fig. 8B, C). In contrast, A20 knockdown increased HcRed fluorescence level (Fig. 8B, C). Taken together, our data demonstrate that A20 negatively regulates constitutive NF-κB activation via its DUB and ligase activity in cultured neurons.

2.7 A20 regulation of spine remodeling requires NF-κB

We finally examined whether the A20 regulation of dendritic spines is mediated through NF-κB signaling. When transfected into cultured hippocampal neurons, both C103A and C624/C627A failed to decrease dendritic protrusions or mushroom spine densities, a characteristic feature of wild-type A20 (Fig. 8D-F). Since both the DUB and E3 ligase activity of A20 are required for the NF-κB signaling, these data suggest that NF-κB activation mediates A20 remodeling of dendritic spines.

To more directly test this hypothesis, we examined the effects of A20 knockdown on dendritic spine density in the presence or absence of a GFP-tagged NF-κB inhibitor (GFP-IκBα) (Boehm et al., 2007) in transfected neurons in culture. IκBα binds p50/p65 dimer (representing NF-κB) and prevents them from translocating to the nucleus to regulate gene expression, and inhibiting IκBα liberates p50/p65 (Chen, 2005; Chen and Sun, 2009). As expected, shA20 significantly increased total spine density, which was completely abolished by co-expression of GFP-IκBα (Fig. 8G, H). These data suggest that A20 negatively regulates dendritic spine density in a NF-κB activation-dependent manner.

3. Discussion

Here we identify the ubiquitin editing enzyme A20/TNFAIP3 as a potent regulator of dendritic spine remodeling and synapse efficacy in neurons. In the canonical NF-κB signaling pathway in the immune system, activation of cytokine receptors (e.g. TNFα and interleukin receptors) results in recruitment of adaptor proteins and ubiquitin E2 and E3 enzymes (TRAF2, TRAF6, and UBC13) to the receptor and synthesis of K63-polyUb chains, leading to activation of TGFβ-activated kinase 1, which activates the IKK complex, resulting in phosphorylation, ubiquitination, and degradation of IκBα and its removal from the p50/p65 dimer. Released NF-κB then translocates to the nucleus where it regulates gene transcription (Chen, 2005; Chen and Sun, 2009). A20 suppresses NF-κB activation by cleaving K63-polyUb chains from several substrates in this pathway, terminating their signaling, by inhibiting interactions between UBC13 and TRAF2 and TRAF6, and by triggering K48 ubiquitination and degradation of UBC13 (Ma and Malynn, 2012; Shembade et al., 2010; Wertz et al., 2004). Our results demonstrate that A20 and NF-κB, key components of this classical immune pathway, operate autonomously in neurons to regulate remodeling of CNS connections.

The presence of A20 in neurons and the PSD and its developmental expression profile suggest a role in synapse development, function, and/or plasticity. Indeed, A20 overexpression reduces dendritic arborization and decreases mushroom, stubby and thin spine sizes and densities (Fig. 2), whereas A20 knockdown increases the sizes and densities of mushroom and stubby spines (Fig. 3). In less mature neurons, A20 overexpression also reduces mushroom spine density but does not significantly alter stubby and thin spines. In the mouse brain in vivo, A20 overexpression and knockdown decrease and increase, respectively, mushroom and stubby spine densities, but spared thin spine densities. The lack of complete consistency between overexpression and knockdown experiments, i.e. they do not always produce entirely consistent results in all aspects of the analysis, is likely due to variations in the extent of gene manipulations, different ages of neurons under examination, and in vitro vs. in vivo settings. In addition, A20 overexpression and knockdown decrease and increase, respectively, the total protein levels of PSD-95 and GluA1. Thus, A20 generally limits dendritic branching and spine formation, especially for the more mature mushroom spines which are consistently regulated. This idea is further supported by the higher intensity of PSD-95 and GluA1 clusters as well as a significantly larger mEPSC amplitude in A20 knockdown neurons, which suggests that synaptic strength is increased when A20 is depleted. It is likely that A20 regulation of synaptic strength occurs primarily at postsynaptic sites since A20 knockdown did not affect mEPSC frequency. However, the unaltered mEPSC frequency yet higher spine densities in A20 knockdown neurons and mouse brains are not readily reconcilable, but one possible mechanism is that some spines formed as a result of A20 depletion may be non-functional. This issue needs further investigation. Together, our data indicates that A20 negatively regulates dendritic spine formation structurally and synaptic strength functionally.

Our study suggests that one mechanism by which A20 remodels the synapse is through regulation of nuclear NF-κB signaling. Initially and primarily studied in inflammation and immune responses, NF-κB also is present and constitutively active in mammalian

excitatory neurons and is rapidly induced by diverse stimuli, exerting potent regulations on dendritic arborization, synaptogenesis, synaptic scaling, and behavioral adaptation under physiological (such as learning and memory) and disease (such as addiction and depression) conditions (Kaltschmidt and Kaltschmidt, 2009; Meffert and Baltimore, 2005; Robison and Nestler, 2011). Increasing evidence indicates that NF-κB is localized at synapses locally and, upon activation by neuronal activity or other stimuli, translocates to the nucleus and induces expression of target genes to orchestrate transcription-dependent structural, functional, and behavioral plasticity (Meffert and Baltimore, 2005). Our findings that A20 localizes at synapses, suppresses neuronal NF-κB activation, and inhibits dendritic spine formation in a NF-κB-dependent manner is consistent with the role of NF-κB in dendritic arborization and synaptogenesis during development and activity-dependent plasticity (Boersma et al., 2011; Dresselhaus et al., 2018; Gutierrez et al., 2005). It is conceivable that A20 regulation of synapse remodeling can be achieved in part by NF-κB-mediated transcription and translation of target genes, including PSD-95 (Boersma et al., 2011) and perhaps yet to be determined spine cytoskeleton elements.

Alternatively, A20-mediated spine remodeling may involve direct protein ubiquitination, degradation, scaffolding and/or trafficking locally in the PSD. Ubiquitination has emerged as a major mechanism in synapse and circuit plasticity. Activity-dependent ubiquitination, presumably linked via K48-polyUb chains and subsequent degradation of synaptic proteins by the proteasome is believed to lead to remodeling and plasticity of synapses (Bingol and Sheng, 2011; DiAntonio and Hicke, 2004; Mabb and Ehlers, 2010). In particular, proteasomes are localized in hippocampal neuron dendrites and are recruited to spines by neuronal activity (Bingol et al., 2010). Plasticity-inducing activity changes cause UPS-dependent degradation of many PSD proteins (Ehlers, 2003) including several major synaptic scaffolds that play crucial roles in synapse strength (Colledge et al., 2003; Ehlers, 2003; Pak and Sheng, 2003; Shin et al., 2012; Tsai et al., 2012). An increasing number of E3 ubiquitin ligases (George et al., 2018) including Parkin (Helton et al., 2008), Ube3A (Avagliano Trezza et al., 2019; Yashiro et al., 2009), APC (Cdh1) (Fu et al., 2011), and Triad3A (Mabb et al., 2014), and DUBs including UCH-L1 (Cartier et al., 2009), USP8 (Kerrisk Campbell and Sheng, 2018), and USP14 (Chen et al., 2009) have been shown to regulate activity-dependent UPS remodeling of synapses, neural circuits, and behavioral plasticity. Furthermore, proteasome-independent ubiquitination and related enzymes have also been found to regulate glutamate receptor function and synapse remodeling (Huo et al., 2015; Kramer et al., 2010; Lin et al., 2011; Lussier et al., 2012; Pavlopoulos et al., 2011; Scudder et al., 2014). Our recent study shows that K63-linked ubiquitination of PSD-95 mediated by K63-specific E3 ligase TRAF6 and DUB CYLD regulates protein-protein interactions and the scaffolding capability of PSD-95 in the PSD, influencing synapse maturation, function, and plasticity (Ma et al., 2017). Here, the identification of A20, a dual K48 E3 ligase and K63 DUB, as a regulator of synapse remodeling provides new insights about potential roles of distinct ubiquitin linkages in synapse and circuit plasticity. Whether A20 deubiquitinates and/or ubiquitinates specific synaptic proteins such as PSD-95, GluA1, and cytoskeletal components as direct substrates, and whether or not ubiquitin chain editing is involved to regulate the level and/or activity of these proteins will require further investigation.

A20 point mutants deficient in either DUB or the E3 ligase activity lost the remodeling and NF-κB modulation capabilities of wild-type A20 protein, indicating that both enzyme activities are required. This is consistent with potential involvement of ubiquitin chain editing, a process by which K63-polyUb chains are first removed from a substrate followed with the conjugation of K48-polyUb chains to the same substrate (Grabbe et al., 2011; Newton et al., 2008). The only known ubiquitin enzyme that can accomplish this is A20 (Ma and Malynn, 2012). An established substrate for A20 is RIP1 (Wertz et al., 2004), which can potentially mediate A20-suppression of nuclear NF-κB activation to regulate target gene transcription to control synapse remodeling. However, it is not absolutely necessary for A20 to exert its synapse remodeling effects via ubiquitin chain editing on the same substrates, and it may directly ubiquitinate/deubiquitinate certain proteins in the PSD locally as mentioned above.

In summary, our results demonstrate that in neurons, A20-NF-κB pathway represents a regulatory mechanism of synaptic remodeling and plasticity. Due to the important status of A20 and NF-κB in mediating immune and inflammatory signaling, and given that pathological neuroinflammation is common in many neuropsychiatric and neurodegenerative diseases (Duman et al., 2016; Estes and McAllister, 2015; Perry et al., 2010; Weiner and Selkoe, 2002) and can potentially remodel the brain during development and through adulthood, the present work may help understand the underlying molecular and cellular mechanisms.

4. Experimental Procedure

Animals:

C57BL/6J mice were bred in-house in standard laboratory conditions. Timed pregnant Sprague Dawley (SD) rats were purchased from Taconic Biosciences, Inc (#1566440, RRID:RGD1566440). Animal care and protocols were approved by the Institutional Animal Care and Use Committee (IACUC) of SUNY Upstate Medical University.

Antibodies:

Primary antibodies used: A20 (Cell Signaling, #5630, RRID: AB_10698880, IF: 1:100), PSD-95 (Cell Signaling, #3450, RRID: AB_2292883), PSD-95 (Santa Cruz, #32290, RRID: AB_628114, IF: 1:50), β-Actin (Santa Cruz, #47778, RRID: AB_2714189), Synapsin I (Millipore, #1543, RRID: AB_2200400), c-Myc (Santa Cruz, #40, RRID: AB_627268), GluA1-NT (Millipore, #2263, RRID: AB_11212678, IF: 1:100–300), NF-κB p65 (Santa Cruz, #8008, RRID: AB_628017, IF: 1:300), phospho-NF-κB p65-S536 (Cell Signaling, #3033, RRID: AB_331284, IF: 1:300), IκBα (Cell Signaling, #4814, RRID: AB_390781), phospho-IκBα-S32 (Cell Signaling, #2859, AB_561111), and Ubc13 (ProSci, #3373, RRID: AB_741284). Secondary antibodies used: HRP conjugated goat anti-mouse IgG (Invitrogen, #62–6520, RRID: AB_2533947), HRP conjugated goat anti-rabbit IgG (Invitrogen, #65–6120, RRID: AB_2533967), Alexa Fluor 568 conjugated goat anti-mouse IgG (Invitrogen, A-11004, RRID: AB_2534072), Alexa Fluor 568 conjugated goat anti-rabbit IgG (Invitrogen, A-11036, RRID: AB_10563566), and Alexa Fluor 647 conjugated goat anti-mouse IgG (Invitrogen, A-21236, RRID: AB_2535805).

Cell culture:

HEK293FT (Invitrogen, R70007, RRID:CVCL 6911) cells were grown and maintained in DMEM supplemented with 10% fetal bovine serum. LipoD293 reagent was used to transfect HEK293FT cells. Primary cortical or hippocampal neurons were prepared from embryonic day 18–19 pregnant SD rats. Dissociated neurons were plated at a density of 5×10^5/ml on 24-well plates, 0.5 ml per well with or without a 100 μg/ml poly-D-lysine (Sigma-Aldrich, P7886)-coated coverslip. For the NF-κB luciferase assay, neurons were plated at a density of 2×10^6/ml on poly-D-lysine-coated 24-well plates. Neurons were maintained in Neurobasal medium supplemented with 2 mM L-glutamine, antibiotics, and B27 supplement. Calcium phosphate was used to transfect neurons.

DNA constructs:

pEGFP-C1-A20 was from Yihong Ye (Addgene, #22141). pCMV-V5-A20 (mouse) was a gift from Michaela Gack. IκB-HcRed was a gift from Philip Auron. GFP-IκBα was from William Hahn (Addgene, #15263). NF-κB-Luciferase and TK-Renilla plasmids were described previously (Ma et al., 2008). Other DNA constructs were subcloned in-house using V5-A20 as the template: pCMV-Myc-A20, Syn-A20-syn-DsRed, Syn-Myc-GFP-Syn-GFP, Syn-Myc-A20-Syn-GFP, Syn-Myc-A20 C103A-Syn-GFP, and Syn-Myc-A20 C624A, 627A-Syn-GFP. Syn-Myc-hA20-Syn-GFP (rA20) was subcloned using pEGFP-C1-A20 as the template. Syn-GFP-Syn-IκB-HcRed was subcloned using IκB-HcRed as the template. pLL3.7-shLuc was described previously (Ma et al., 2017). We designed three targeting shRNA sequences for A20: #1: 5’-GGAGACAGACACTCGGAACTT-3’, #2: 5’-GTTTGGAATCTGGTTCCAATT-3’, and #3: 5’-GGACTCCCAGGCGTGGGACTT-3’. shA20 #1, #2 and #3 were constructed by cloning the target sequences into PLL3.7. All constructs were verified by DNA sequencing and protein expression.

Virus:

HEK293FT cells were transfected with pHCMV-G, pCMV-Δ8.9, and pLL3.7-shLuc, pLL3.7-shA20#1, Syn-Myc-GFP-Syn-GFP, Syn-Myc-A20-Syn-GFP or Syn-Myc-hA20-Syn-GFP to produce lentivirus. The supernatant was harvested 48 hrs post transfection, filtered, and concentrated. Virus solution was used to infect cultured rat neurons in vitro and mouse hippocampal neurons in vivo. For in vitro infection, low titer lentivirus (1μl/well, 1×10^6 function units/ml) was added to the medium of cultured neurons. For in vivo infection, high titer lentivirus (1μl/injection site, 1×10^7 function units/ml) was injected into the mouse brain.

Stereotaxic injection and brain section preparation:

C57BL/6J mice of both sexes at postnatal day 15 (P15) were randomly selected, anesthetized and placed on a stereotaxic frame. The lentiviruses expressing Syn-Myc-GFP-Syn-GFP, Syn-Myc-A20-Syn-GFP, U6-shLuc-CMV-GFP or U6-shA20-CMV-GFP were injected bilaterally into the hippocampi as described previously (Ma et al., 2017). Mice were sacrificed at P30 and brains were cryosectioned at 150 um thickness for confocal imaging of dendritic morphology.

Western blotting:

Cultured rat neurons and mouse brains were lysed in RIPA buffer (50 mM Tris-HCL pH 7.4, 0.1% SDS, 1% NP-40, 0.25% deoxycholic acid, 150 mM NaCl, 1 mM EDTA) in the presence of 1 mM PMSF and protease inhibitor cocktail. Total protein concentrations were measured with a Pierce BCA protein assay kit. Lysates were resolved by SDS-PAGE gel, and transferred onto a PVDF membrane. After blocking with 2% BSA or 5% fat-free milk, membrane was incubated with a primary antibody at 4°C overnight. After washes the membrane was incubated with appropriate HRP conjugated secondary antibodies at room temperature for 1 hr. Blots were developed with SuperSignal West Femto Maximum Sensitivity Substrate (Thermo Fisher, #34095). Images were acquired with the ChemiDoc MP system. If necessary, blots were stripped with a stripping buffer and re-probed with indicated antibodies. Protein bands were quantified by ImageJ.

Subcellular fractions of rat brain homogenates were prepared by continuous sucrose gradient centrifugation as described (Ma et al., 2017). A20 in each fraction was detected by Western blotting.

NF-κB luciferase reporter assay:

Neurons were transfected with NF-κB-Luciferase and TK-Renilla reporter plasmids plus indicated A20-related plasmids. Neurons were processed for Luciferase assay at DIV16 following the manufacture's protocol for Dual-Luciferase® Reporter (DLR™) Assay System (Promega, E1910). Luciferase levels were measured as relative light units (RLUs). We typically achieve ~10% co-transfection efficiency in high-density neuron cultures for these experiments.

Immunostaining, confocal microscopy, and image analysis:

Cultured neurons were fixed in 4% paraformaldehyde and 5% sucrose in PBS for 15 min, permeabilized with 0.3% Tween-20 in PBST for 20 min, blocked with 1% BSA for 1 hr, and incubated with indicated primary antibodies at 4°C overnight followed by incubation with secondary antibodies conjugated with appropriate Alexa Fluor dyes for 1 hr. For labeling of surface GluA1 (sGluA1) receptors, neurons at DIV20 were live fed with anti-GluA1-NT antibody in warm medium for 30 min in a 5% CO2 incubator, washed 3x with medium, fixed in 4% paraformaldehyde and 5% sucrose in PBS for 5 min, and incubated with Alexa Fluor 568 second antibody diluted in 1% BSA at 1:250 at room temperature for 1 hr. After wash, neurons or brain sections were mounted on glass slides.

Confocal microscopy and image analysis of dendritic spines and clustering of PSD-95 and GluA1 were done similarly as previously described (Ma et al., 2017) with minor modifications. For confocal microscopy, image stacks along the z axis were acquired using a Leica TCS SP5 Spectral Confocal Microscope (Leica Microsystems) fitted with a 40X objective at pixel resolutions of 512 × 512. Image acquisition settings were kept the same for all scans when fluorescence quantification was required. For quantifications of fluorescence intensity, outlines of selected areas were carefully traced and fluorescence signal was then measured for the traced areas. Maximum projection images were analyzed.

Neurite complexity was analyzed by the Sholl plugin embedded in ImageJ (Ferreira et al., 2014) according to (Binley et al., 2014). For quantifications of dendritic spine density, GFP or DsRed-expressing dendrites (one segment per neuron) from DIV19–20 neurons transfected with indicated plasmids were first selected using NeuronStudio software. Numbers of total, mushroom, stubby, and thin spines per 10 μm were counted. Spine types were automatically classified by NeuronStudio using the default setting and criteria implemented in the software. Spine head area was measured from carefully traced region as the spine size. Individual cluster or spine measurements were first grouped and averaged per neuron. Means from multiple neurons in the same group were then averaged to obtain a population mean and presented as mean ± SEM. Similar quantifications were done for dendritic protrusion density from DIV16 neurons (which had more filopodia but fewer spines) expressing A20 mutants and controls (Fig. 8D-F). Dendritic arborization and spine analyses were done blindly. For quantifications of PSD-95, surface GluA1, and total GluA1 clustering in neurons transfected with shA20 or shLuc control, the fluorescence intensities of carefully traced clusters on randomly selected dendrites were measured. One or more dendrites were selected from individual neurons and the average fluorescence intensity was calculated for each segment, and all the segments were then averaged to derive the mean ± SEM. For quantifications of p65, p-p65, and IκBα-HcRed fluorescence signals, soma and proximal processes of individual neurons (confined in a 50 μm × 50 μm square with the soma located approximately at the center as shown in Figs. 7D and 8B) transfected with indicated plasmids were traced based on the GFP expression in the “green” channel and the fluorescence intensities for the traced areas measured at the “red or blue” channel. Endogenous A20 immunofluorescence (Fig. S1B,C) from non-transfected and shLuc/GFP- or shA20/GFP-transfected neurons was quantified from carefully traced (in red or green channels) soma and processes of the neuron.

For data processing, background fluorescence of an image was first measured from a signal-free region on the same image and subtracted, while necessary. Fluorescence signals were measured as pixel intensities defined as integrated pixel intensities (i.e. total 8-bit intensity values across all pixels contained in traced areas) in specific channels divided by the total number of pixels. All groups to be compared were run simultaneously using the same batch of cells. More detailed procedures have been described previously (Ma et al., 2017).

Electrophysiology:

Cultured hippocampal neurons were infected with lentivirus expressing shLuc, shA20 or shA20/rA20 at DIV7. At DIV12~14, coverslips were removed from 24-well plates and transferred to the recording chamber with artificial cerebrospinal fluid (ACSF) containing (in mM) 126 NaCl, 1.2 NaH_2PO_4, 2.5 KCl, 1.2 $MgCl_2$, 25 $NaHCO_3$, 11 D-Glucose, 2.5 $CaCl_2$ (pH 7.4 by pre-saturated with 95% O_2 and 5% CO_2). Tetrodotoxin (TTX; 1 μm, a sodium channel blocker), APV (50 μm, a NMDAR blocker), and picrotoxin (100 μm, a $GABA_A$ receptor blocker) were included in the ACSF during recording. Whole-cell patch-clamp recordings were made with patch pipettes filled with an intracellular solution containing (in mM) 130 K-gluconate, 8 NaCl, 10 HEPES, 0.4 EGTA, 5 QX-314 (lidocaine N-ethyl bromide), 2 Mg-ATP, 0.25 GTP-Tris (pH 7.3), with the membrane potential held at −60 mV. Recordings were performed at ambient temperature using a Molecular Devices

Multiclamp 700B amplifier. Data were collected with pClamp 10 (Molecular Devices). The threshold for automated detections of miniature excitatory synaptic current (mEPSC) event was 5 pA, which was near the background noise level. This threshold was adopted to ensure every event was picked up by the software, followed by a careful manual inspection to ensure each event was a true mEPSC. The amplitude and frequency of mEPSCs were analyzed with Mini Analysis Program (Synaptosoft, Version 6.0.7). Recordings were done with the electrophysiologist blinded to the genotypes of the cells. Cells that met the following criteria were excluded from analysis: i) the baseline was randomly fluctuating (presumably due to unstable cell membrane) that prevented faithful detections of mini events. ii) extremely low mEPSC frequency - despite stable recording for several minutes, there was no detectable events or the number of events were too few to reach 0.01 Hz.

Statistics:

All data were presented as mean ± SEM. Unpaired Student's t test was used to compare two independent variables. One-way ANOVA with appropriate post-hoc test was used to compare multiple variables. mEPSC distributions were analyzed by Kolmogorov-Smirnov test. Statistical significance was set at 0.05.

Supplementary Material

Refer to Web version on PubMed Central for supplementary material.

Acknowledgements

We thank Michaela U. Gack and Philip. E. Auron for providing plasmids, and members of the laboratory and Peter Koch for comments and discussions. This study was supported by NIH grants, MH106489, NS093097, DA032283, and RR026761 (W.-D.Y.).

Abbreviations:

ACSF	artificial cerebrospinal fluid
AMPA	α-amino-3-hydroxy-5-methyl-4-isoxazolepropionic acid
DIV	days in vitro
DUB	deubiquitinase
GABA	gamma-aminobutyric acid
IKK	inhibitor of nuclear factor kappa-B kinase
IκB	inhibitor of nuclear factor kappa-B
IKK-γ	inhibitor of nuclear factor kappa-B kinase subunit gamma
mEPSC	miniature excitatory postsynaptic current
NEMO	NF-κB essential modulator
NMDA	N-methyl-D-aspartate

p65/RelA	NF-κB p65 subunit/REL-associated protein
polyUb	polyubiquitin
PSD-95	postsynaptic density-95
NF-κB	nuclear factor kappa-light-chain-enhancer of activated B cells
OTU	ovarian tumor
RIP1	receptor-interacting protein 1
TNFα	tumor necrosis factor α
TNFAIP3	TNFα induced protein 3
TRAF	TNF receptor-associated factor
TTX	tetrodotoxin
UBC13	ubiquitin-conjugating enzyme E2 13
UPS	ubiquitin proteasome system

References

Avagliano Trezza R, Sonzogni M, Bossuyt SNV, Zampeta FI, Punt AM, van den Berg M, Rotaru DC, Koene LMC, Munshi ST, Stedehouder J, et al. (2019). Loss of nuclear UBE3A causes electrophysiological and behavioral deficits in mice and is associated with Angelman syndrome. Nat Neurosci 22, 1235–1247. [PubMed: 31235931]

Bingol B, and Sheng M (2011). Deconstruction for reconstruction: the role of proteolysis in neural plasticity and disease. Neuron 69, 22–32. [PubMed: 21220096]

Bingol B, Wang CF, Arnott D, Cheng D, Peng J, and Sheng M (2010). Autophosphorylated CaMKIIalpha acts as a scaffold to recruit proteasomes to dendritic spines. Cell 140, 567–578. [PubMed: 20178748]

Binley KE, Ng WS, Tribble JR, Song B, and Morgan JE (2014). Sholl analysis: a quantitative comparison of semi-automated methods. J Neurosci Methods 225, 65–70. [PubMed: 24485871]

Boehm JS, Zhao JJ, Yao J, Kim SY, Firestein R, Dunn IF, Sjostrom SK, Garraway LA, Weremowicz S, Richardson AL, et al. (2007). Integrative genomic approaches identify IKBKE as a breast cancer oncogene. Cell 129, 1065–1079. [PubMed: 17574021]

Boersma MC, Dresselhaus EC, De Biase LM, Mihalas AB, Bergles DE, and Meffert MK (2011). A requirement for nuclear factor-kappaB in developmental and plasticity-associated synaptogenesis. J Neurosci 31, 5414–5425. [PubMed: 21471377]

Bosanac I, Wertz IE, Pan B, Yu C, Kusam S, Lam C, Phu L, Phung Q, Maurer B, Arnott D, et al. (2010). Ubiquitin binding to A20 ZnF4 is required for modulation of NF-kappaB signaling. Mol Cell 40, 548–557. [PubMed: 21095585]

Cartier AE, Djakovic SN, Salehi A, Wilson SM, Masliah E, and Patrick GN (2009). Regulation of synaptic structure by ubiquitin C-terminal hydrolase L1. J Neurosci 29, 7857–7868. [PubMed: 19535597]

Catrysse L, Vereecke L, Beyaert R, and van Loo G (2014). A20 in inflammation and autoimmunity. Trends Immunol 35, 22–31. [PubMed: 24246475]

Chen PC, Qin LN, Li XM, Walters BJ, Wilson JA, Mei L, and Wilson SM (2009). The proteasome-associated deubiquitinating enzyme Usp14 is essential for the maintenance of synaptic ubiquitin levels and the development of neuromuscular junctions. J Neurosci 29, 10909–10919. [PubMed: 19726649]

Chen ZJ (2005). Ubiquitin signalling in the NF-kappaB pathway. Nat Cell Biol 7, 758–765. [PubMed: 16056267]

Chen ZJ, and Sun LJ (2009). Nonproteolytic functions of ubiquitin in cell signaling. Mol Cell 33, 275–286. [PubMed: 19217402]

Colledge M, Snyder EM, Crozier RA, Soderling JA, Jin Y, Langeberg LK, Lu H, Bear MF, and Scott JD (2003). Ubiquitination regulates PSD-95 degradation and AMPA receptor surface expression. Neuron 40, 595–607. [PubMed: 14642282]

DiAntonio A, and Hicke L (2004). Ubiquitin-dependent regulation of the synapse. Annu Rev Neurosci 27, 223–246. [PubMed: 15217332]

Dresselhaus EC, Boersma MCH, and Meffert MK (2018). Targeting of NF-kappaB to Dendritic Spines Is Required for Synaptic Signaling and Spine Development. J Neurosci 38, 4093–4103. [PubMed: 29555853]

Duman RS, Aghajanian GK, Sanacora G, and Krystal JH (2016). Synaptic plasticity and depression: new insights from stress and rapid-acting antidepressants. Nat Med 22, 238–249. [PubMed: 26937618]

Ehlers MD (2003). Activity level controls postsynaptic composition and signaling via the ubiquitin-proteasome system. Nat Neurosci 6, 231–242. [PubMed: 12577062]

Elias GM, and Nicoll RA (2007). Synaptic trafficking of glutamate receptors by MAGUK scaffolding proteins. Trends Cell Biol 17, 343–352. [PubMed: 17644382]

Estes ML, and McAllister AK (2015). Immune mediators in the brain and peripheral tissues in autism spectrum disorder. Nat Rev Neurosci 16, 469–486. [PubMed: 26189694]

Ferreira TA, Blackman AV, Oyrer J, Jayabal S, Chung AJ, Watt AJ, Sjostrom PJ, and van Meyel DJ (2014). Neuronal morphometry directly from bitmap images. Nat Methods 11, 982–984. [PubMed: 25264773]

Fu AK, Hung KW, Fu WY, Shen C, Chen Y, Xia J, Lai KO, and Ip NY (2011). APC(Cdh1) mediates EphA4-dependent downregulation of AMPA receptors in homeostatic plasticity. Nat Neurosci 14, 181–189. [PubMed: 21186356]

George AJ, Hoffiz YC, Charles AJ, Zhu Y, and Mabb AM (2018). A Comprehensive Atlas of E3 Ubiquitin Ligase Mutations in Neurological Disorders. Front Genet 9, 29. [PubMed: 29491882]

Grabbe C, Husnjak K, and Dikic I (2011). The spatial and temporal organization of ubiquitin networks. Nat Rev Mol Cell Biol 12, 295–307. [PubMed: 21448225]

Guedes RP, Csizmadia E, Moll HP, Ma A, Ferran C, and da Silva CG (2014). A20 deficiency causes spontaneous neuroinflammation in mice. J Neuroinflammation 11, 122. [PubMed: 25026958]

Gutierrez H, Hale VA, Dolcet X, and Davies A (2005). NF-kappaB signalling regulates the growth of neural processes in the developing PNS and CNS. Development 132, 1713–1726. [PubMed: 15743881]

Gutierrez H, O'Keeffe GW, Gavalda N, Gallagher D, and Davies AM (2008). Nuclear factor kappa B signaling either stimulates or inhibits neurite growth depending on the phosphorylation status of p65/RelA. J Neurosci 28, 8246–8256. [PubMed: 18701687]

Haglund K, and Dikic I (2005). Ubiquitylation and cell signaling. EMBO J 24, 3353–3359. [PubMed: 16148945]

Harper JW, Ordureau A, and Heo JM (2018). Building and decoding ubiquitin chains for mitophagy. Nat Rev Mol Cell Biol 19, 93–108. [PubMed: 29358684]

Helton TD, Otsuka T, Lee MC, Mu Y, and Ehlers MD (2008). Pruning and loss of excitatory synapses by the parkin ubiquitin ligase. Proc Natl Acad Sci U S A 105, 19492–19497. [PubMed: 19033459]

Hershko A, and Ciechanover A (1998). The ubiquitin system. Annu Rev Biochem 67, 425–479. [PubMed: 9759494]

Huo Y, Khatri N, Hou Q, Gilbert J, Wang G, and Man HY (2015). The deubiquitinating enzyme USP46 regulates AMPA receptor ubiquitination and trafficking. J Neurochem 134, 1067–1080. [PubMed: 26077708]

Husnjak K, and Dikic I (2012). Ubiquitin-binding proteins: decoders of ubiquitin-mediated cellular functions. Annu Rev Biochem 81, 291–322. [PubMed: 22482907]

Kaltschmidt B, and Kaltschmidt C (2009). NF-kappaB in the nervous system. Cold Spring Harb Perspect Biol 1, a001271. [PubMed: 20066105]

Kerrisk Campbell M, and Sheng M (2018). USP8 Deubiquitinates SHANK3 to Control Synapse Density and SHANK3 Activity-Dependent Protein Levels. J Neurosci 38, 5289–5301. [PubMed: 29735556]

Komander D, Clague MJ, and Urbe S (2009). Breaking the chains: structure and function of the deubiquitinases. Nat Rev Mol Cell Biol 10, 550–563. [PubMed: 19626045]

Kramer LB, Shim J, Previtera ML, Isack NR, Lee MC, Firestein BL, and Rongo C (2010). UEV-1 is an ubiquitin-conjugating enzyme variant that regulates glutamate receptor trafficking in C. elegans neurons. PloS one 5, e14291. [PubMed: 21179194]

Lin A, Hou Q, Jarzylo L, Amato S, Gilbert J, Shang F, and Man HY (2011). Nedd4-mediated AMPA receptor ubiquitination regulates receptor turnover and trafficking. J Neurochem 119, 27–39. [PubMed: 21338354]

Lu W, Shi Y, Jackson AC, Bjorgan K, During MJ, Sprengel R, Seeburg PH, and Nicoll RA (2009). Subunit composition of synaptic AMPA receptors revealed by a single-cell genetic approach. Neuron 62, 254–268. [PubMed: 19409270]

Lussier MP, Herring BE, Nasu-Nishimura Y, Neutzner A, Karbowski M, Youle RJ, Nicoll RA, and Roche KW (2012). Ubiquitin ligase RNF167 regulates AMPA receptor-mediated synaptic transmission. Proc Natl Acad Sci U S A 109, 19426–19431. [PubMed: 23129617]

Ma A, and Malynn BA (2012). A20: linking a complex regulator of ubiquitylation to immunity and human disease. Nat Rev Immunol 12, 774–785. [PubMed: 23059429]

Ma Q, Ruan H, Peng L, Zhang M, Gack MU, and Yao WD (2017). Proteasome-independent polyubiquitin linkage regulates synapse scaffolding, efficacy, and plasticity. Proc Natl Acad Sci U S A 114, E8760–E8769. [PubMed: 28973854]

Ma Q, Zhou L, Shi H, and Huo K (2008). NUMBL interacts with TAB2 and inhibits TNFalpha and IL-1beta-induced NF-kappaB activation. Cell Signal 20, 1044–1051. [PubMed: 18299187]

Mabb AM, and Ehlers MD (2010). Ubiquitination in postsynaptic function and plasticity. Annu Rev Cell Dev Biol 26, 179–210. [PubMed: 20604708]

Mabb AM, Je HS, Wall MJ, Robinson CG, Larsen RS, Qiang Y, Correa SA, and Ehlers MD (2014). Triad3A regulates synaptic strength by ubiquitination of Arc. Neuron 82, 1299–1316. [PubMed: 24945773]

Meffert MK, and Baltimore D (2005). Physiological functions for brain NF-kappaB. Trends Neurosci 28, 37–43. [PubMed: 15626495]

Mukhopadhyay D, and Riezman H (2007). Proteasome-independent functions of ubiquitin in endocytosis and signaling. Science 315, 201–205. [PubMed: 17218518]

Newton K, Matsumoto ML, Wertz IE, Kirkpatrick DS, Lill JR, Tan J, Dugger D, Gordon N, Sidhu SS, Fellouse FA, et al. (2008). Ubiquitin chain editing revealed by polyubiquitin linkage-specific antibodies. Cell 134, 668–678. [PubMed: 18724939]

Pak DT, and Sheng M (2003). Targeted protein degradation and synapse remodeling by an inducible protein kinase. Science 302, 1368–1373. [PubMed: 14576440]

Parisi C, Napoli G, Amadio S, Spalloni A, Apolloni S, Longone P, and Volonte C (2016). MicroRNA-125b regulates microglia activation and motor neuron death in ALS. Cell Death Differ 23, 531–541. [PubMed: 26794445]

Pavlopoulos E, Trifilieff P, Chevaleyre V, Fioriti L, Zairis S, Pagano A, Malleret G, and Kandel ER (2011). Neuralized1 activates CPEB3: a function for nonproteolytic ubiquitin in synaptic plasticity and memory storage. Cell 147, 1369–1383. [PubMed: 22153079]

Peluffo H, Gonzalez P, Acarin L, Aris A, Beyaert R, Villaverde A, and Gonzalez B (2013). Overexpression of the nuclear factor kappaB inhibitor A20 is neurotoxic after an excitotoxic injury to the immature rat brain. Neurol Res 35, 308–319. [PubMed: 23336395]

Perry VH, Nicoll JA, and Holmes C (2010). Microglia in neurodegenerative disease. Nat Rev Neurol 6, 193–201. [PubMed: 20234358]

Pranski EL, Van Sanford CD, Dalal NV, Orr AL, Karmali D, Cooper DS, Costa N, Heilman CJ, Gearing M, Lah JJ, et al. (2012). Comparative distribution of protein components of the

A20 ubiquitin-editing complex in normal human brain. Neurosci Lett 520, 104–109. [PubMed: 22634524]

Robison AJ, and Nestler EJ (2011). Transcriptional and epigenetic mechanisms of addiction. Nat Rev Neurosci 12, 623–637. [PubMed: 21989194]

Scudder SL, Goo MS, Cartier AE, Molteni A, Schwarz LA, Wright R, and Patrick GN (2014). Synaptic strength is bidirectionally controlled by opposing activity-dependent regulation of Nedd4-1 and USP8. J Neurosci 34, 16637–16649. [PubMed: 25505317]

Shembade N, Ma A, and Harhaj EW (2010). Inhibition of NF-kappaB signaling by A20 through disruption of ubiquitin enzyme complexes. Science 327, 1135–1139. [PubMed: 20185725]

Shin SM, Zhang N, Hansen J, Gerges NZ, Pak DT, Sheng M, and Lee SH (2012). GKAP orchestrates activity-dependent postsynaptic protein remodeling and homeostatic scaling. Nat Neurosci 15, 1655–1666. [PubMed: 23143515]

Skaug B, Chen J, Du F, He J, Ma A, and Chen ZJ (2011). Direct, noncatalytic mechanism of IKK inhibition by A20. Mol Cell 44, 559–571. [PubMed: 22099304]

Traynelis SF, Wollmuth LP, McBain CJ, Menniti FS, Vance KM, Ogden KK, Hansen KB, Yuan H, Myers SJ, and Dingledine R (2010). Glutamate receptor ion channels: structure, regulation, and function. Pharmacol Rev 62, 405–496. [PubMed: 20716669]

Tsai NP, Wilkerson JR, Guo W, Maksimova MA, DeMartino GN, Cowan CW, and Huber KM (2012). Multiple autism-linked genes mediate synapse elimination via proteasomal degradation of a synaptic scaffold PSD-95. Cell 151, 1581–1594. [PubMed: 23260144]

Vereecke L, Beyaert R, and van Loo G (2009). The ubiquitin-editing enzyme A20 (TNFAIP3) is a central regulator of immunopathology. Trends Immunol 30, 383–391. [PubMed: 19643665]

Wang KZ, Galson DL, and Auron PE (2010). TRAF6 is autoinhibited by an intramolecular interaction which is counteracted by trans-ubiquitination. J Cell Biochem 110, 763–771. [PubMed: 20512936]

Wang X, Deckert M, Xuan NT, Nishanth G, Just S, Waisman A, Naumann M, and Schluter D (2013). Astrocytic A20 ameliorates experimental autoimmune encephalomyelitis by inhibiting NF-kappaB- and STAT1-dependent chemokine production in astrocytes. Acta Neuropathol 126, 711–724. [PubMed: 24077734]

Weiner HL, and Selkoe DJ (2002). Inflammation and therapeutic vaccination in CNS diseases. Nature 420, 879–884. [PubMed: 12490962]

Wenthold RJ, Petralia RS, Blahos J II, and Niedzielski AS (1996). Evidence for multiple AMPA receptor complexes in hippocampal CA1/CA2 neurons. J Neurosci 16, 1982–1989. [PubMed: 8604042]

Wertz IE, O'Rourke KM, Zhou H, Eby M, Aravind L, Seshagiri S, Wu P, Wiesmann C, Baker R, Boone DL, et al. (2004). De-ubiquitination and ubiquitin ligase domains of A20 downregulate NF-kappaB signalling. Nature 430, 694–699. [PubMed: 15258597]

Yamada T, Yang Y, and Bonni A (2013). Spatial organization of ubiquitin ligase pathways orchestrates neuronal connectivity. Trends Neurosci 36, 218–226. [PubMed: 23332798]

Yashiro K, Riday TT, Condon KH, Roberts AC, Bernardo DR, Prakash R, Weinberg RJ, Ehlers MD, and Philpot BD (2009). Ube3a is required for experience-dependent maturation of the neocortex. Nat Neurosci 12, 777–783. [PubMed: 19430469]

Yu L, Miao H, Hou Y, Zhang B, and Guo L (2006). Neuroprotective effect of A20 on TNF-induced postischemic apoptosis. Neurochem Res 31, 21–32. [PubMed: 16474993]

Highlights:

- The ubiquitin-editing enzyme A20 is expressed in rodent brain pyramidal neurons and is localized in dendritic spines and postsynaptic densities.
- A20 reduces dendritic complexity and inhibits dendritic spine formation in hippocampal neurons.
- A20 inhibits glutamatergic scaffold and receptor clustering and synaptic efficacy in cultured hippocampal neurons.
- A20 suppresses NF-κB activation in cultured hippocampal neurons.
- A20 regulates dendritic spine remodeling in a NF-κB-dependent mechanism.

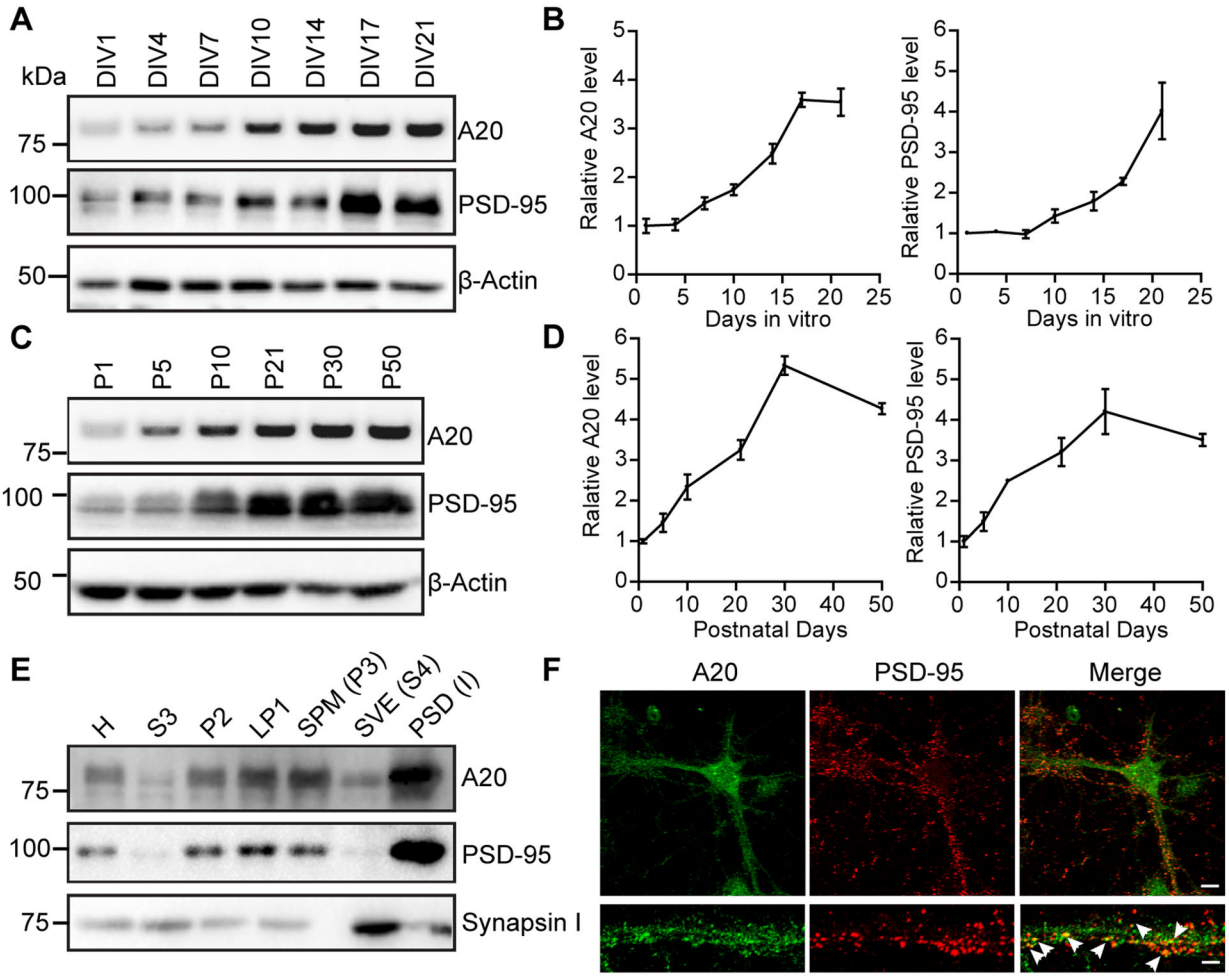

Figure 1.

A20 expression in rodent neurons and brains. ***A***, Western blot detections of A20 in cultured rat cortical neurons at different DIVs. *B*, Quantifications of relative expression levels of A20 and PSD-95 from ***A***. n = 3 independent experiments. ***C***, Western blot detections of A20 in mouse cortices at different postnatal days. ***D***, Quantifications of relative expression levels of A20 and PSD-95 from ***C***. n = 3 independent experiments. ***E***, Western blot detections of A20 expression in subcellular fractions of the rat brain. H: homogenate, S3: cytosol, P2: crude synaptosomal membrane, LP1: synaptosome fraction, SPM (P3): synaptic plasma membrane, SVE (S4): synaptic vesicle enriched, PSD (I): PSD fraction after one Triton X-100 extraction. ***F***, Rat neuronal cultures were fixed and immunostained with A20 and PSD-95 antibodies at DIV19 and imaged with confocal microscopy. Arrowheads, colocalized PSD-95 (red) and A20 (green) clusters. Scale bars, 10 μm (above) and 2 μm (below).

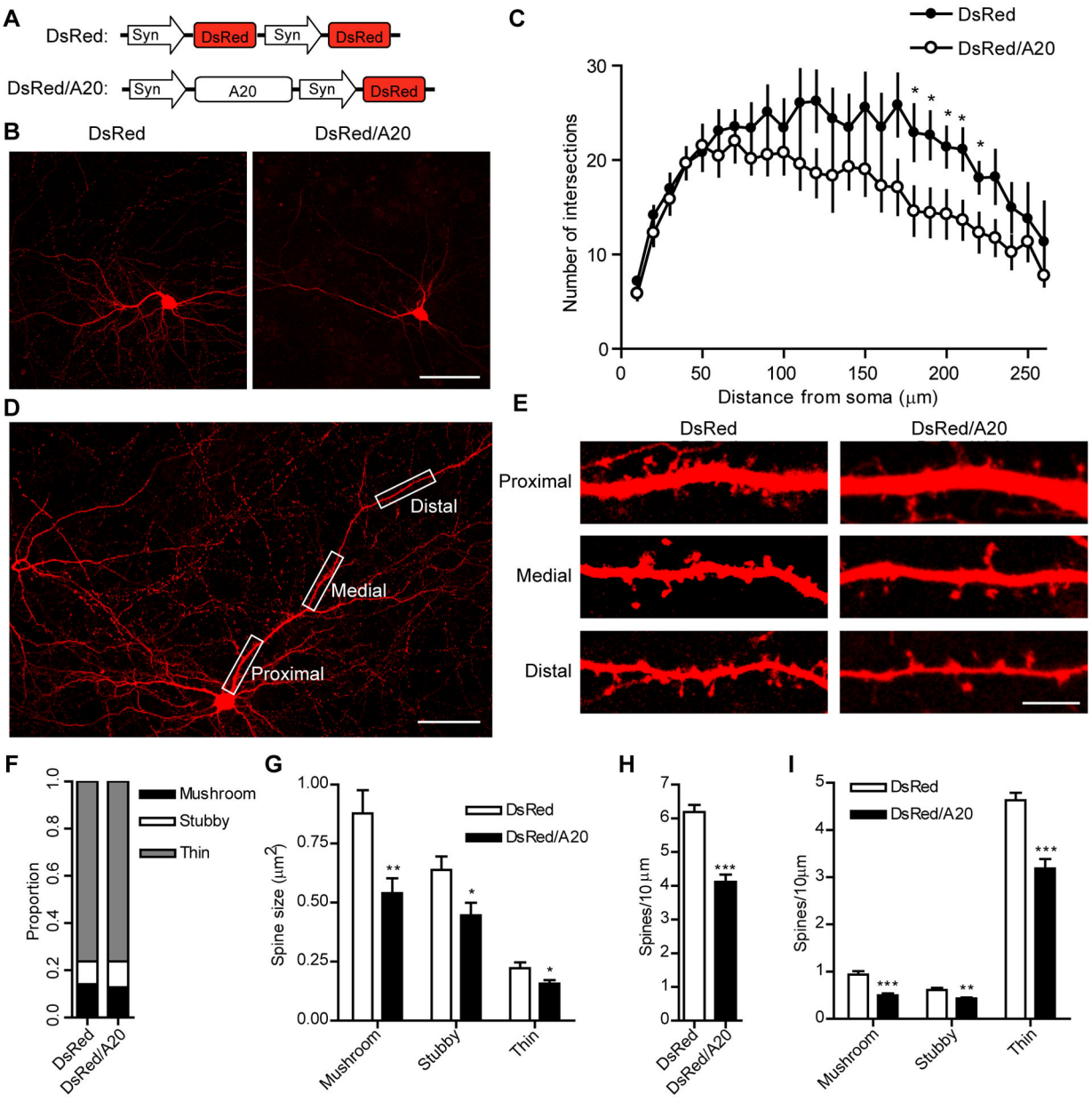

Figure 2.

Effects of A20 overexpression on neuronal morphology. ***A***, DsRed/A20 and DsRed constructs used. Syn, synapsin I promoter. ***B***, Representative cultured hippocampal neurons expressing DsRed or DsRed/A20. Scale bars, 100 μm. ***C***, Sholl analysis of dendritic arborization and complexity. n =11 and 9 cells in DsRed and DsRed/A20 groups, respectively, from at least 2 batches of neuronal cultures from different embryos. *p < 0.05; Student's t-tests. ***D***, A representative cultured hippocampus neuron illustrating the proximal, medial, and distal segments of dendrites. Refer **Experimental Procedures** for classifications. Scale bar, 50 μm. ***E***, Representative proximal, medial, and distal dendritic branches at higher magnification showing individual spines on dendritic shafts. Scale bar, 5 μm. ***F***, Comparison of proportions of mushroom, stubby, and thin spine numbers in

control and A20 overexpression groups. ***G***, Summary of head sizes for three spine types as indicated. ***H***, ***I***, Summary of total (***H***) and classified (***I***) spine densities. Spines from proximal, medial, and distal regions were combined in each group for (***F-I***). n =15 and 13 cells for Syn-DsRed transfected and Syn-DsRed-Syn-A20 transfected groups, respectively. Data in (***D-I***) were from at least 3 separate batches of neuronal cultures from different embryos. *p < 0.05; **p < 0.01; ***p < 0.001; unpaired t tests.

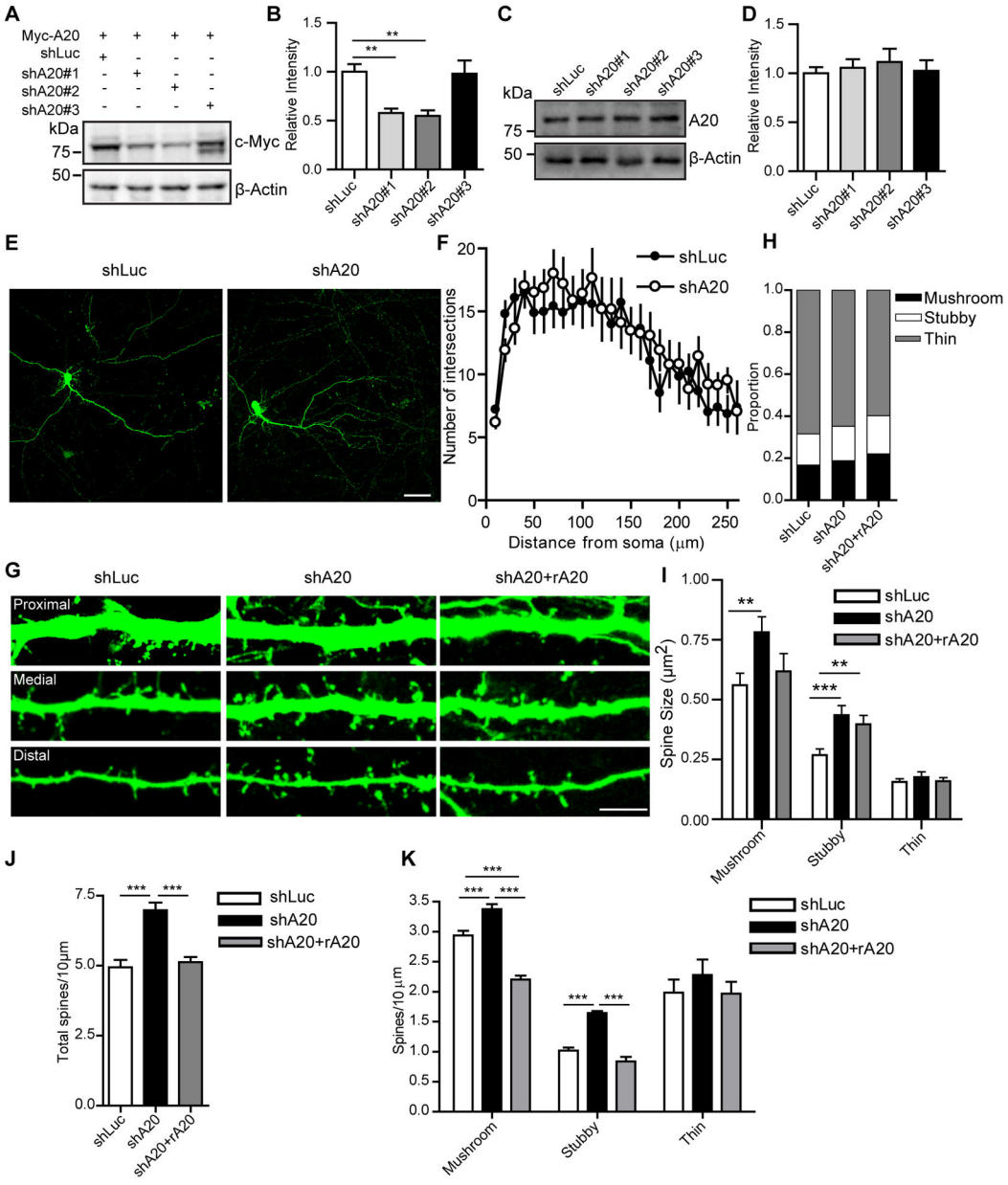

Figure 3.

Effects of A20 knockdown on neuronal morphology. ***A***, Western blot testing of knockdown efficiencies of three shA20 constructs in HEK293FT cells cotransfected with indicated plasmids. ***B***, Quantifications from ***A***. n = 5 independent immunoblotting experiments performed on lysates from different batches of cell cultures. **p < 0.01; one-way ANOVA with post hoc Dunnett's multiple comparison tests. ***C***, lack of effect of shA20 constructs on the endogenous A20 in HEK293FT cells transfected with indicated shRNAs. ***D***, Quantifications from ***C***. n = 3 independent immunoblotting experiments performed on lysates from different batches of cell cultures. ***E***, Representative cultured hippocampal neurons expressing shLuc or shA20. Scale bar, 50 μm. ***F***, Sholl analysis of dendritic arborization and complexity. n = 14 and 16 cells in shLuc and shA20 groups, respectively,

from at least 2 batches of neuronal cultures from different embryos. ***G***, Representative proximal, medial, and distal dendritic branches showing individual spines on dendritic shafts. Scale bar, 5 μm. ***H***, Proportions of three spine types in control, A20 knockdown, and RNAi-resistant rescue groups. ***I***, Quantifications of the sizes of three spine types from ***G***. ***J, K***, Summaries of total and classified spine densities. n=15, 14, 13 in shLuc, shA20, and shA20/rA20 groups, respectively. Spines from proximal, medial, and distal regions were combined in each group for (***I-K***). Data in (***G-K***) were collected from at least 3 separate batches of neuronal cultures from different embryos. *p < 0.05, *p < 0.01, ***p < 0.001; one-way ANOVA with post hoc Tukey's multiple comparison tests.

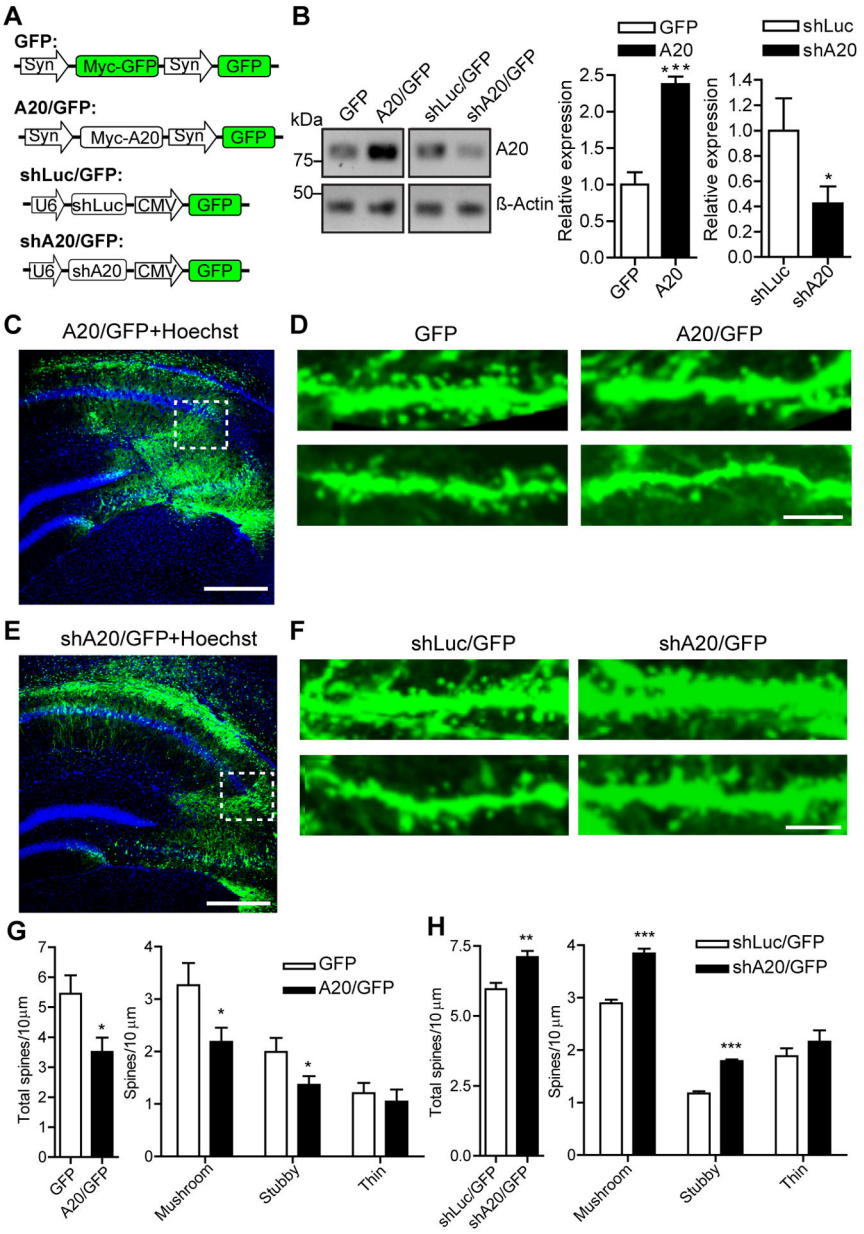

Figure 4.

Effects of A20 manipulations in dendritic spine densities in vivo. ***A***, Constructs used for lentivirus packaging. ***B***, Western blots (left) and quantifications (right) showing knockdown and overexpression efficiencies of various lentiviruses used in stereotaxic injections. n = 6, 5, 3, and 5 independent immunoblotting experiments on separate neuronal cultures for GFP, A20, shLuc, and shA20 groups, respectively. *p < 0.05, ***p < 0.001; unpaired t tests. ***C, E***, Representative hippocampal regions infected with lentivirus expressing A20/GFP (***C***) or shA20/GFP (***E***). Nuclei were labeled with Hoechst 33342. Scale bars, 350 μm. ***D***, ***F***, Representative dendritic branches at higher magnifications showing individual spines on dendritic shafts in GFP, A20/GFP, shLuc/GFP, or shA20/GFP infected neurons. Dotted boxes indicate where dendrites in ***D*** and ***F*** were sampled. Scale bars, 5 μm. ***G***,

Quantifications of densities of total and classified spines from ***D***. n = 8 in each group (left) and n = 13 and 15 for GFP and A20/GFP, respectively (right). ***H***, Quantifications of densities of total and classified spines from ***F***. n = 13 and 19 in shLuc and shA20 groups, respectively (left), and n = 15 and 14 in shLuc and shA20 groups, respectively (right). n = 3 mice used in each group. *p < 0.05, ***p < 0.001; unpaired t tests.

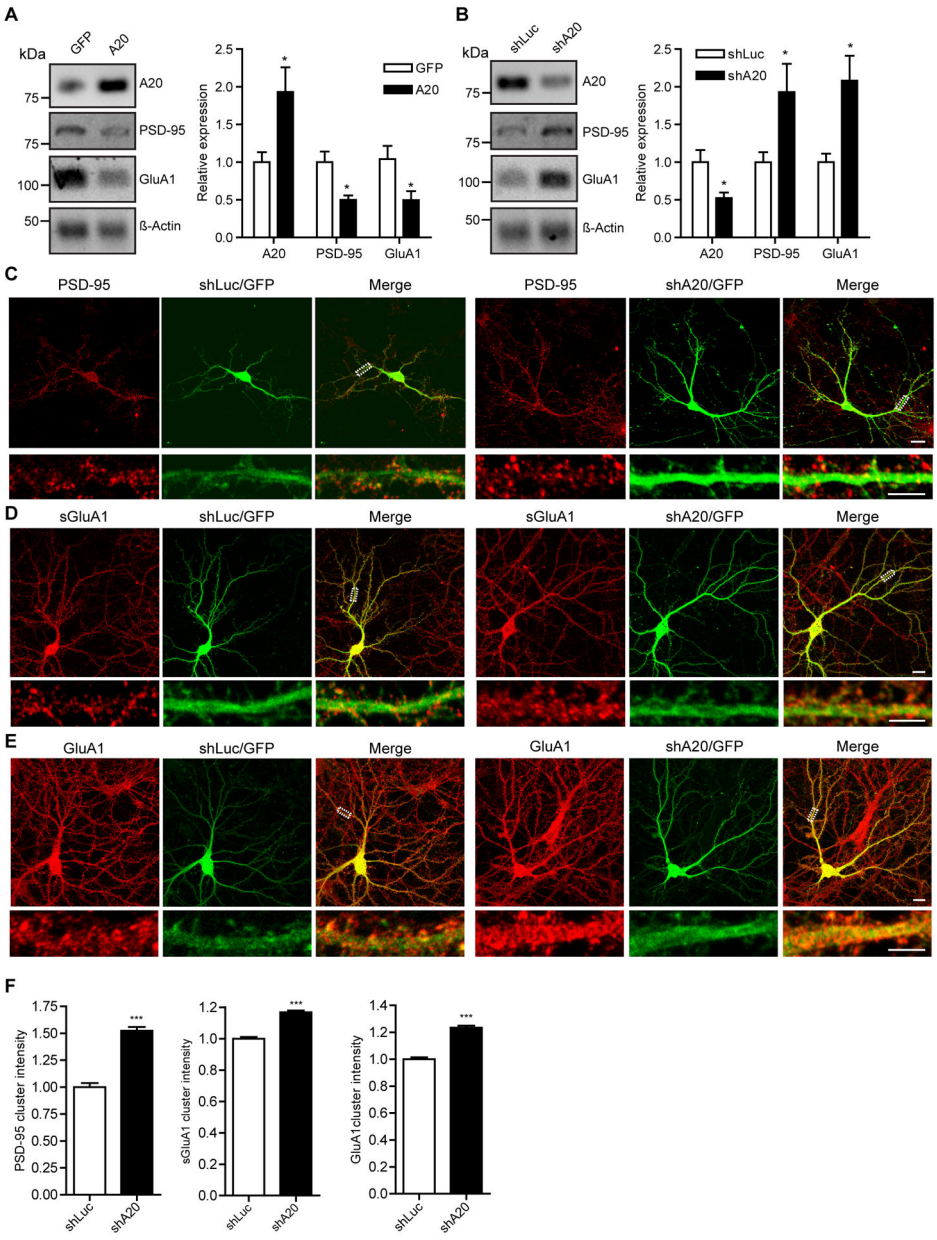

Figure 5.

A20 regulation of PSD-95 and GluA1 clustering. ***A***, Western blot (left) and quantifications (right) showing that A20 overexpression reduces PSD-95 and GluA1 total levels. n = 4–5 independent experiments. *p < 0.05; unpaired t tests. ***B***, Western blot (left) and quantifications (right) showing that A20 knockdown increases PSD-95 and GluA1 total levels. n = 3–5 independent experiments. *p < 0.05; unpaired t tests. ***C***, PSD-95 clusters (red) in shLuc/GFP or shA20/GFP expressing neurons. Scale bars, 20 μm (above) and 5 μm (below). ***D***, sGluA1 clusters (red) in A20 knockdown and control neurons. Scale bars, 20 μm (above) and 5 μm (below). ***E***, Total GluA1 clusters (red) in A20 knockdown and control neurons. Scale bars, 20 μm (above) and 5 μm (below). Boxes indicate where the dendritic segments were zoomed in at a higher magnification. ***F***, Quantifications of PSD-95, GluA1,

and sGluA1 cluster intensities in ***C-E***. n = 63, 51, 232, 242, 144, and 151 dendritic branches, respectively, for PSD-95, sGluA1, and GluA1 clusters in shLuc and shA20 neurons in the order shown. ***P < 0.001, unpaired t test.

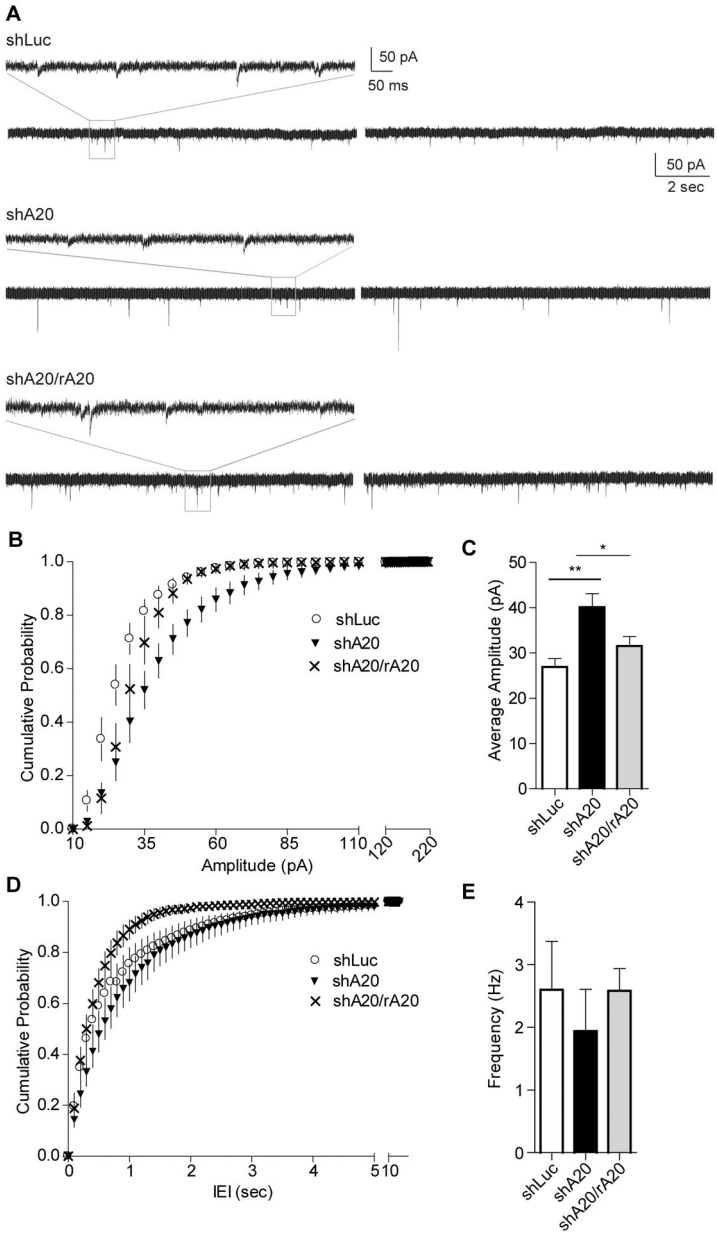

Figure 6.

A20 knockdown enhances synapse strength in cultured hippocampal neurons. ***A***, Representative traces of mEPSCs recorded from shLuc, shA20, and RNAi-resistant rescue A20 lentivirus infected neurons. Boxed regions were zoomed in to show higher temporal resolution current records. ***B***, Cumulative probabilities of mEPSC amplitude. ***C***, Average mEPSC amplitude. ***D***, Cumulative probabilities of mEPSC inter-event intervals (IEI). ***E***, Average mEPSC frequency. n = 10, 8, 9 cells for shLuc, shA20, and shA20/rA20 groups, respectively. Cells were from 3, 2, and 4 separate neuronal cultures from different embryos. *p < 0.05, **p < 0.01, one-way ANOVA with post hoc Tukey's multiple comparison tests.

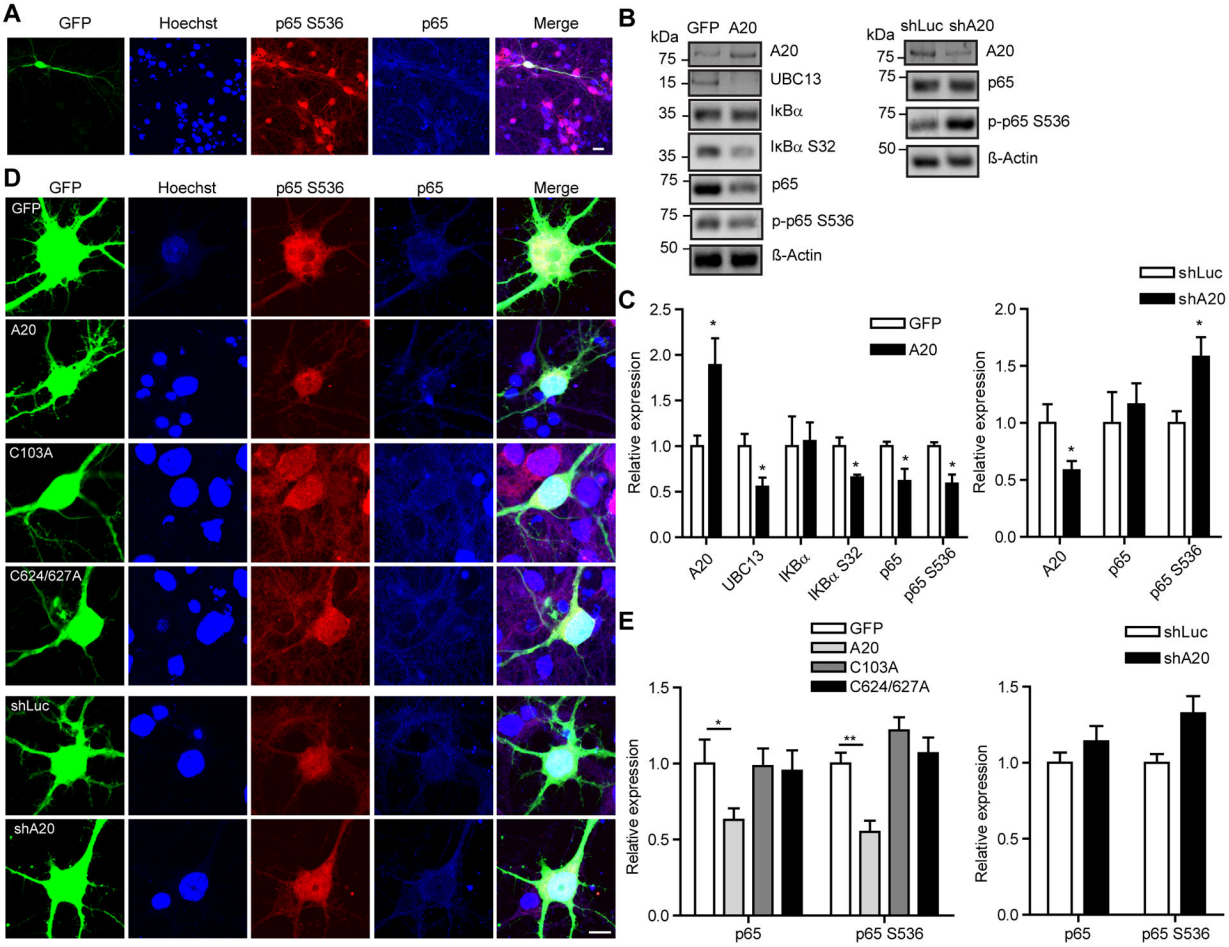

Figure 7.

A20 regulates p-p65 S536 levels in cultured neurons. ***A***, High levels of constitutive p-p65 S536 in cultured neurons. Nuclei were labeled with Hoechst 33342. Scale bar, 20 μm. ***B***, Western blots showing effects of A20 overexpression (left) and knockdown (right) on indicated proteins in the NF-κB pathway in neurons infected with GFP, A20, shLuc, or shA20 lentiviruses at DIV16. ***C***, Quantifications of ***B***. n = 3–7 independent experiments. *p < 0.05, unpaired t-tests. ***D***, Immunofluoresence of p65 and p-p65 S536 in neurons transfected (DIV7) with indicated plasmids and examined at DIV16. Nuclei were labeled with Hoechst 33342. Scale bar, 10 μm. ***E***, Quantifications of p65 and p-p65 S536 levels from ***D***. n = 10, 10, 8, 8, 8, and 8 cells for GFP, A20, C103A, C624/C627A, shLuc, and shA20 groups, respectively. *p < 0.05, **p < 0.01; One-way ANOVA followed by post hoc Dunnett's multiple comparison tests for overexpression (left); unpaired t tests for knockdown (right).

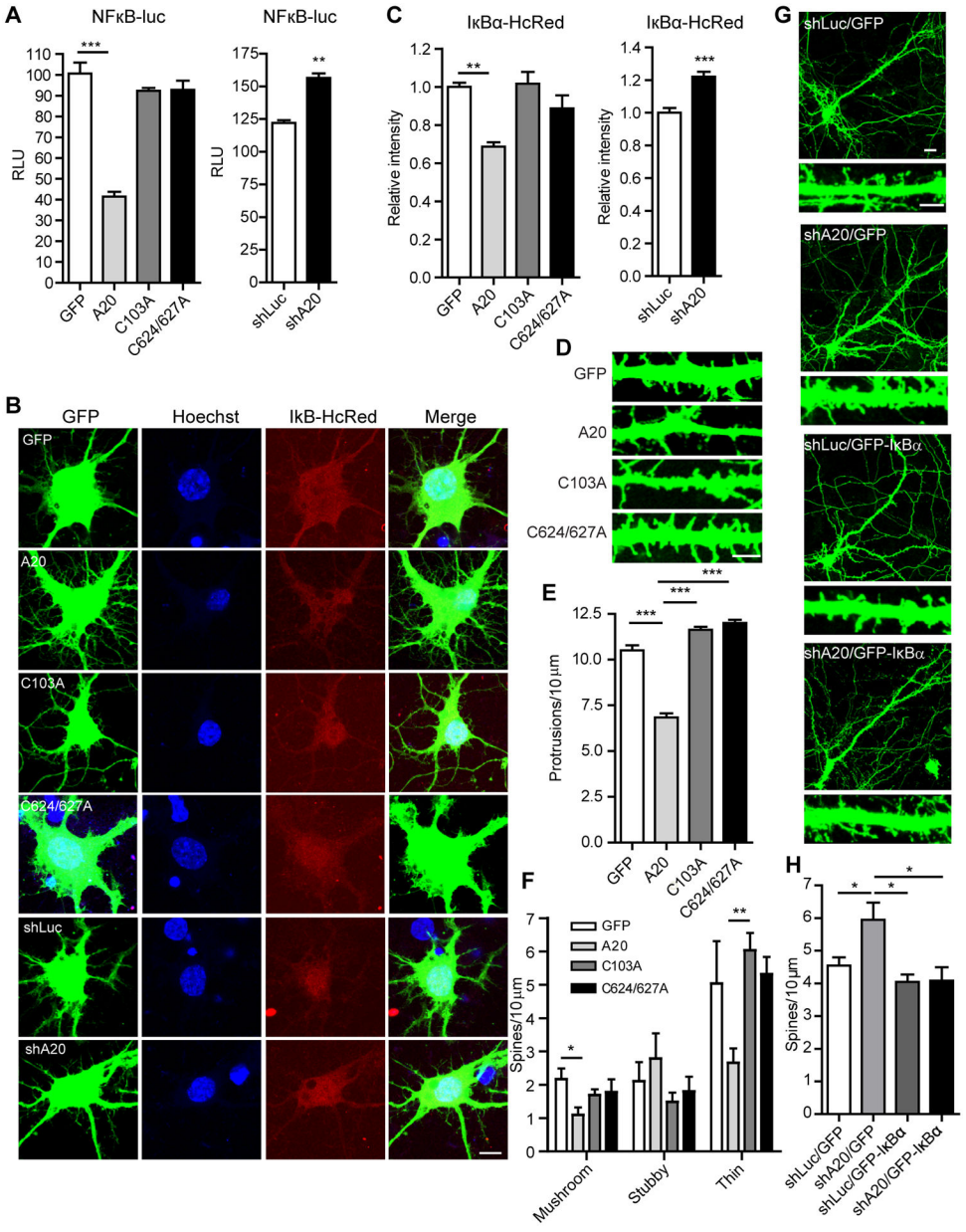

Figure 8.

A20 regulates NF-κB activation in cultured neurons and dendritic spine remodeling in a NF-κB-dependent manner. ***A***, Luciferase assay quantifying NF-κB activation (at DIV16) in neurons transfected (at DIV7) with NF-κB-luciferase reporters plus indicated constructs. **p < 0.01, ***p < 0.001. one-way ANOVA with post hoc Dunnett's multiple comparison tests (left) and unpaired t tests (right). ***B***, Representative fluorescence images of neurons (DIV16) transfected (DIV7) with IκB-HcRed reporter plus indicated constructs. Nuclei were labeled with Hoechst 33342. Scale bar, 10 μm. ***C***, Quantifications of IκB-HcRed signals from ***B***. n = 9, 9, 8, 7, 9, and 8 cells for GFP, A20, C103A, C624/627A, shLuc, and shA20 groups, respectively. **p < 0.01, ***p < 0.001; one-way ANOVA with post hoc Dunnett's multiple comparison tests (left) and unpaired t tests (right). ***D***, Representative

dendrite branches of GFP, A20, and mutants from DIV16 neurons. Scale bar, 5 μm. ***E, F***, Summaries of total protrusions (used for younger neurons with more filopodia and fewer spines) and classified spine densities from ***D***. n=6, 7, 8, and 6 cells in GFP, A20, C103A, and C624/627A groups, respectively. *p < 0.05, **p < 0.01, ***p < 0.001; one-way ANOVA with post hoc Tukey's multiple comparison tests. ***G***, Representative whole-cell images and dendrite segments of shLuc/GFP, shA20/GFP, shLuc/GFP-IκBα, and shA20/GFP-IκBα transfected neurons (DIV20). Scale bars, 10 μm (above) and 5 μm (below). ***H***, quantifications of dendritic spine densities from ***G***. n = 15, 15, 9, and 9 cells for shLuc/GFP, shA20/GFP, shLuc/GFP-IκBα, and shA20/GFP-IκBα groups, respectively. *p < 0.05; one-way ANOVA with post hoc Tukey's multiple comparison tests.